Mineralogical and microstructural evolution of Portland cement paste/argillite interfaces at 70 °C – Considerations for diffusion and porosity properties

Philippines Lalan, Alexandre Dauzères, Laurent de Windt, Juuso Sammaljärvi, Daniele Bartier, Isabelle Techer, Valéry Detilleux, Marja Siitari-Kauppi

Mineralogical and microstructural evolution of Portland cement paste/argillite interfaces at 70 °C – Considerations for diffusion and porosity properties

Philippines Lalan[a,b], Alexandre Dauzères[a,*], Laurent De Windt[b], Juuso Sammaljärvi[c], Danièle Bartier[d], Isabelle Techer[e], Valéry Detilleux[f], Marja Siitari-Kauppi[c]

[a] Institute of Radiation Protection and Nuclear Safety (IRSN)/PRP-DGE/SRTG/LETIS, BP 17, 92262 Fontenay-aux-Roses cedex, France
[b] MINES ParisTech, PSL Research University, Centre de Géosciences, 77300 Fontainebleau, France
[c] Laboratory of Radiochemistry HYRL, Department of Chemistry, PO Box 55, 00014, University of Helsinki, Finland
[d] CNRS UMR 7566, Université de Lorraine, BP 70239, 54506 Vandœuvre-lès-Nancy, France
[e] Univ. Nîmes, EA 7352 CHROME, rue du Dr Georges Salan, 30021 Nîmes, France
[f] Bel V, 148 Rue Walcourt, 1070 Anderlecht, Belgium

ARTICLE INFO

Keywords:
CEM I
Degradation
Diffusion
Microstructure
Temperature
Tournemire
Waste management

ABSTRACT

A Portland cement (CEM I) paste was poured onto an argillite disk in diffusion cells with reservoirs filled by alkaline water and argillite pore water. The system evolution was followed over the course of 415 days. The imposed temperature of 70 °C affected the mineralogy (precipitation of crystallized C-S-H) and mechanical strength of the interface that became brittle over time. The interface consisted of a calcite/tobermorite/C-A-S-H layer, whose thickness increased at a growth rate of 0.3 µm/d. Contrary to calcite crusts that formed in immersion tests or when hardened cement was placed in contact with argillite, this layer had no significant effect on the diffusion properties during the one-year duration of the experiment due to its microporous structure and rather small thickness (100 µm). The argillite mineralogy was altered over 100 µm. In the cement paste, the total porosity decreased because carbonation was enhanced with temperature, which counterbalanced the effect of decalcification over 400 µm.

1. Introduction

Over the last decades, interest has grown regarding the geochemical behaviour of cementitious materials in a clayey environment. Due to the favourable radionuclide containment properties of argillaceous rocks, disposal facilities for radioactive waste in natural clayey environments are considered to be a highly valuable option in several countries, such as in Belgium, France and Switzerland. On the other hand, cementitious materials are interesting for ensuring the mechanical stability of galleries and future radioactive waste cells. The contact created between the clayey rock and the concrete is known to inevitably lead to an alkaline plume spreading from the concrete towards the host rock, while a multi-ionic attack occurs from the clayey pore water against the cementitious material side. These chemical perturbations strongly impact the microstructure and diffusion properties. Consequently, their global abilities of containment, especially at their interfaces, could be altered. Additionally, heat is another parameter to consider. Indeed, in the French disposal concept, the radioactive wastes that emit heat are expected to cause a transient increase in the temperature of up to 70 °C within the concrete plugs located in the high-level waste cells. The same phenomenon would occur to a lesser degree in the intermediate long-lived waste cells. The temperature effect on interfaces between waste disposal components is, therefore, a key parameter to study while assessing the performance of radioactive waste disposals.

In the literature, studies have focused mainly on the physicochemical evolution of clay under alkaline conditions, and not on the physical interfaces between two materials. Only a few studies have discussed interactions at the interface between cement binders and claystone. Such interfaces were created at ambient temperature by pouring cement mixes into boreholes [1–5] or by putting disks of material into contact in transport cells [6,7]. Even fewer laboratory studies have focused on the impact of such a temperature on interfaces between cement-based materials and clays (e.g., [7–8]). Mineralogical changes

* Corresponding author.
E-mail addresses: alexandre.dauzeres@irsn.fr (A. Dauzères), laurent.de_windt@mines-paristech.fr (L. De Windt), daniele.bartier@univ-lorraine.fr (D. Bartier), isabelle.techer@unimes.fr (I. Techer), valery.detilleux@belv.be (V. Detilleux).

in the materials, i.e., precipitation and dissolution of solid phases, would have consequences on the microstructure and volume of the pores. The evolution of microstructure and spatial distribution of porosity during degradation are both important factors that must be understood to accurately model the mass transfer diffusion within cementitious porous media or at material interfaces (e.g., [9]), and subsequently, to extend the modelling evolution of engineered barriers to the long-term [10,11].

Although the understanding of the microstructural evolution at interfaces is crucial, the literature is less extended on these questions because the study of microstructural evolution is rather tricky and requires specific analytical tools. This paper aims to fill the knowledge gap regarding the evolution of geochemical, microstructural and diffusional properties of clay/cementitious binder interfaces under full water saturation and a representative temperature of 70 °C. Cell experiments were performed using a Portland Cement (OPC) binder and the Toarcian argillite extract out of the underground research laboratory (URL) in Tournemire (France). The cell experiments were performed under well-controlled conditions and were launched in complement to an in situ experiment setup in the Tournemire URL. The same time of interaction was chosen for both set-ups [12].

The cement paste was poured onto the argillite disk and was placed in the middle of the cell. Reservoirs were filled with alkaline water and argillite pore water, respectively, on both the cement binder side and argillite side. The purpose of these reservoirs is to simulate the chemical effect of a thicker material and to facilitate indirect access to the evolution of the pore water composition of each material. Three cells running in parallel were successively dismantled over the course of one year to determine the mineralogical and microstructural evolution. The microstructure was investigated by X-ray micro-tomography and C14-PMMA autoradiography. The first technique provides information on the spatial distribution and value of the macro (capillary) porosity, whereas the latter enables access to the total connected porosity.

2. Materials and methods

2.1. Materials

2.1.1. Clayey rock

Samples of argillite (claystone) were collected out of the IRSN underground research laboratory (URL) of Tournemire (Aveyron, France). Tournemire URL is located in a tunnel that crosses a 250 m thick formation of Toarcian and Domerian ages [13]. Core samples 52 mm of diameter were extracted from the Upper Toarcian level and were cut into 1 cm-thick disks. The disk section was almost parallel to the stratigraphy. The Upper Toarcian argillite is mainly composed of clay minerals including illite, an illite/smectite mixed layer, kaolinite and chlorite. Minor minerals include quartz, carbonates, such as calcite and dolomite, feldspar and pyrite [14]. Approximately 1 wt% of organic matter was measured [15]. Argillite pore water is fossilised seawater containing mainly NaCl and sulfates with a pH of approximately 7.8 [13,14]. Main features are summarized in Table 1.

Porosity varies between 7 and 15% [14,16]. The hydraulic conductivity of the argillite is very low (10^{-13} m/s) [13]. The effective diffusion coefficient perpendicular to stratigraphy (D_e) is 7.7×10^{-12} m^2/s at 20 °C [17].

2.1.2. OPC paste

The selected cement binder was sulfate resisting Portland cement from Val d'Azergues (CEM I 52.5 N), provided by Lafarge. Hydration was performed with a water/cement mass ratio of 0.42. Cement paste characterization by XRD confirmed the presence of portlandite, C-S-H, Si-katoite ($Ca_3Al_2SiO_4(OH)_8$), ettringite, traces of calcite and anhydrous species. More details on the characterization are given in Lalan et al. [12]. The connected total porosity measured by the water method was approximately 35% (± 1%) and was approximately 30% (± 3%) measured by the polymethyl methacrylate (PMMA) method. The hydraulic conductivity was not measured, but this parameter is known to be low for hydrated cement pastes with a W/C of 0.4. The effective diffusion was approximately 6×10^{-12} m^2/s at 20 °C. Within the cells, since both materials have low permeability, the mass transport was only driven by diffusion when fully hydrated and because the cells were not submitted to any pressure gradients.

2.1.3. Synthetic pore waters

Four solutions were prepared in the laboratory from salts dissolved in deionised water. The composition of these solutions was chosen to be close to the equilibrium between the material and its pore water at 70 °C. The composition of the argillite synthetic pore water was adapted from Chautard et al. [15,18], where equilibrium was calculated at 60 °C. The composition of the cement paste synthetic pore water was calculated at equilibrium with portlandite, and alkalines were added to reach the concentration measured in a young OPC paste. A second step was necessary to finish preparing the argillite synthetic water in order to obtain the CO_2 partial pressure and pH measured in the rock. For this purpose, a gas composed of 1% CO_2 and 99% N_2 was introduced to the solution until it reached equilibrium. The compositions of these solutions are listed in Table 2.

2.2. Experimental setup and protocol

After being cut, the argillite disks were resaturated by a vapour phase by storing them in an airtight container at 100% relative humidity. To set up the diffusion cell, the first step was to place the materials in the sample holder while ensuring water tightness around the material. To achieve this, a thin rubber seal was placed on the porous plate located at the bottom of the sample holder. The circumference of an argillite disk was beforehand coated with mastic (Resoltech 3030) and then embedded in a thick rubber seal (1 cm thick, 52 mm inner diameter). The circumference of the latter was also coated with mastic, and finally, the entire assemblage was placed into the sample holder. A second thick rubber seal was stuck on the top of the first. After mastic hardening (24 h later), cement paste was poured onto the argillite disk in the central space of the second thick rubber seal to shape (once hardened) a 52 mm diameter and 1 cm thick cement paste disk. After 24 h, the diffusion cell parts were screwed together and the reservoirs were filled with water corresponding to the material in contact. Three diffusion cells were simultaneously prepared using the same cement mix and were then stored in a climatic chamber at 70 °C and 80% of relative humidity. Fig. 1 shows the geometry of the diffusion cells.

Solutions were sampled every 3 days for the first two weeks, then once per week for the following 20 weeks, and finally once every two weeks. Volumes of 2 mL were sampled from the alkaline reservoir, and volumes of 4 mL were sampled from the argillite synthetic water reservoir. After each sampling, each reservoir was refilled with the corresponding initial solution at 70 °C. The experiments were terminated after 76, 202 and 415 days by dismantling the diffusion cells.

Table 1
Mineralogical composition of Tournemire argillite at the underground laboratory depth.

Minerals	Illite	I/S	Kaolinite	Chlorite	Quartz	Carbonates	Feldspar	Pyrite
wt%	15–30	15–35	10–20	≈5	10–20	10–15	≈5	≈3

Table 2
Synthetic pore water compositions used in the reservoirs of diffusion cells.

Argillite water (mmol/L)		Alkaline water (mmol/L)	
$NaHCO_3$	3.6	NaOH	50
Na_2SO_4	8.1	KOH	270
NaCl	1.4	$Ca(OH)_2$	0.6
KCl	0.7		
$CaCl_2$, $2H_2O$	1.7		
$MgCl_2$, $6H_2O$	0.8		

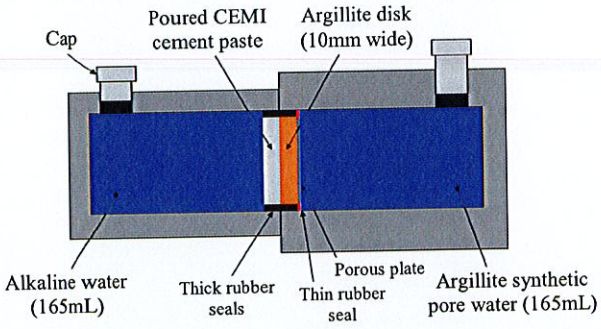

Fig. 1. Scheme of the diffusion cell displaying the cement and argillite disks in contact with the reservoirs filled with alkaline water and argillite pore water.

2.3. Analytical methods

2.3.1. Scanning electron microscopy (SEM-EDS)

Samples were freeze-dried for a week and embedded in epoxy resin. Polished thin-sections centred on the interface were then prepared and coated by carbon. During sample preparation, specific attention was paid to ensure contact between the two faces of the interface. Secondary Electron (SE) observations were performed by Scanning Electron Microscopy (SEM, Hitachi S3500N - IRSN, Fontenay-aux-Roses, France) for mineral morphological information. Chemical characterizations were performed with an energy-dispersive spectrometry (EDS) system that was adapted onto the SEM and was composed of two EDS - Brücker SDD detectors working under a voltage of 15 keV at a working distance of 16 mm. The spot size of the EDS measurement was approximately 1 µm and the SEM-Beam interaction pear was approximately 3 µm in depth.

2.3.2. X-ray diffraction (XRD)

XRD analyses were performed shortly after dismantling the cells and directly on the solid, without drying or embedding the samples into resin [19,20]. Between each measurement, the sample surface was abraded with 350-grain abrasive paper (silicon carbide) and the new surface was analysed. A thickness comparator was used to check the depth of abrasion. The objective was to follow the mineralogical evolution with distance from the interface. Mineralogical data were collected using a PANalytical X'Pert diffractometer with an X'Celerator detector (IMPMC, Paris VI University, France) relying on CuKα radiation (λ = 1.5405 Å). The working voltage and intensity were equal to 40 kV and 40 mA, respectively. The clay section was scanned between 4 and 65° and the cement section between 5 and 60° with a step size of 0.02°, and a time per step of 0.50 s. Phase characterization was performed using EVA software and the PDF database of the International Centre for Diffraction Data (ICDD). Intensities of the characteristic peaks of each phase were directly measured on the solid. Mineralogical profiles were qualitatively built from the intensity values with respect to a control mineral (e.g., C4AF).

2.3.3. X-ray micro-tomography

Analyses were performed on a non-embedded sample with an approximate size of 1.5 × 1.5 × 10 mm using a computed tomography scanner Phoenix Nanotom S (GeoRessources, Université de Lorraine, France). Scans were performed at 90 keV and 125 mA with a voxel size of 0.8 µm in order to optimize contrast between the different mineral phases and the porosity. Once the sample reconstitution had been performed, a porosity profile was obtained using the Avizo 9 software.

2.3.4. C-14 impregnation technique

C-14 PMMA autoradiography is based on measuring the radiation from radioactive elements trapped within the sample. In the chosen configuration, the beta radiation emitted from the C-14 is measured. To produce high-resolution images, the maximal beta energy of this emitter (156 keV) is suitable. The C-14-labelled compound, methyl methacrylate (MMA), can intrude into nanometre-scale pores [21,22], which makes it suitable for analysing nanoporous materials such as clays. The sample is put against an imaging plate and the radiation interacts with the latter. The imaging plate contains BaFBr:Eu photostimulable crystals that undergo an oxidation reaction of Eu(II) to Eu (III) when exposed to beta radiation. This reaction also liberates electrons that are trapped in the bromine vacancies of the crystal lattice. The more the plate receives beta energy, the more electrons are trapped by the bromine vacancies. Once the imaging plate had been scanned, the input is the intensity value of each pixel. The intensity is usually expressed in grey levels (256 levels for 8 bit systems). The local concentration of trapped electrons in the plate is proportional to the grey value intensity. These intensities are converted into corresponding optical densities using Lambert's Law [23–26].

The uncertainties in C-14-PMMA autoradiography arise from errors in physical parameters, calibration parameters and optical density measurements. Mathematical treatment of the error has been presented by Sammartino et al. [27]. Error increases when the measured activities diverge from the linear range of the calibration curve [24]. In this work, the relative error was found to be mostly within 10%, except for very high and very low activity values. Low activity values are more difficult to distinguish from the background, and high activity values suffer saturation. The exposure time of the autoradiograph must, therefore, be chosen carefully. High exposure times usually increase visual contrast, but a larger amount of the autoradiograph shifts to the saturation range, which gives lower porosity values than actually exist. The conclusions from the empirical work and literature are twofold. First, a relative error of 10% could be applied for C-14-PMMA autoradiography. Second, the exposure time had to be chosen to optimize the visual contrast and to have most of the autoradiograph within the linear range of the calibration curve [24,27,28].

2.3.5. Aqueous sample analysis

The pH was directly measured twice in the reservoir; twice per week for the first 15 weeks, and finally once per week. The pH probe used is heating resistant from ambient temperatures to 140 °C (Steamline – SI analytics) and is calibrated at 50 °C. Anion concentrations were measured by ion liquid chromatography using an 861 Advanced Compact IC (Metrohm). Cation and silicon concentrations were measured by ICP-OES (Inductively Coupled Plasma - Optical Emission Spectroscopy) using ICAP 7000 (Thermo Scientific). Additional measurements were performed on the argillite synthetic water samples to obtain the total organic carbon (TOC) and total inorganic carbon (TIC) using a TOC analyser (VarioTOC, ELEMENTAR) for solutions.

2.4. Modelling approach and data

To support the interpretation of experimental diffusion data and porosity evolution, the diffusion of potassium under water-saturated conditions was calculated using the reactive transport code HYTEC [29]. The pore water chemistry and cation exchanges were only considered using the multi-site cation exchange model of Tremosa et al. [14]. The cationic exchange capacity (CEC) of the Tournemire argillite

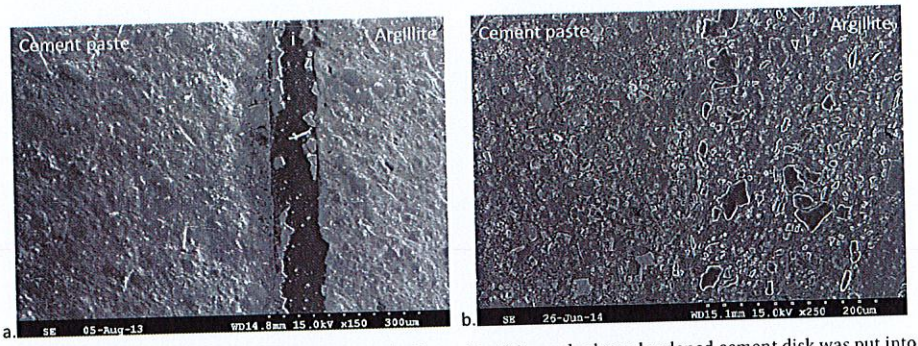

Fig. 2. Very different cement/argillite interfaces are obtained after 2 months depending (a) on whether a hardened cement disk was put into contact with the argillite disk or (b) the cement was directly poured onto the argillite (SEM images in SEB-SE mode, *i* stands for interface).

measured at the tunnel height is 8.64×10^{-2} molc/kg of grain. The geochemical module of HYTEC (CHESS) was also used to build stability phase diagrams using the Thermoddem thermodynamic database [30]. Thermodynamic data for the solid phases were selected from Lalan et al. [12].

3. Results

3.1. Prerequisites

3.1.1. Interface evolution, hardened cement disk versus cement poured into the cell

Prior to the experimental work, the protocol to produce a perfectly joined interface had to be determined. The first attempt consisted of putting together an argillite disk and a hardened cement paste disk. Observation of the polished sections by SEM confirmed that this test protocol did not create a perfect contact between both disks (Fig. 2a). Precipitation of calcite crystals in the interstice was favoured by a void of a few tens of microns. In the present study protocol, the fresh cement mix was directly poured onto an argillite disk within the sample holder. Fig. 2b perfectly illustrates that the interface was sealed, easily identifiable and localizable with this protocol. No mixing zone was observed. In saturated conditions, the formation of calcite crystals at open cement/argillite paste interfaces and in adjacent fractures of argillite had already been demonstrated at 80 °C. Nevertheless, in areas where the interfaces were contiguous, cohesion of the materials was maintained [31]. Thus, an initial gap at the interface favours interface clogging by calcite crust, whereas pouring the cement mix onto the argillite favours diffusive transfer. The second protocol was found to be more representative of disposal conditions and, therefore, chosen for the present study.

3.1.2. Reproducibility in the three diffusion cells

The chemical evolutions of the reservoirs were simultaneously monitored to ensure that the post-mortem analysis of the three diffusion cells could be used as three different phases of the same process. Fig. 3 shows the good reproducibility of the evolution over time of the pH and the potassium concentration in the three cells.

3.2. Mineralogical and microstructural evolution over time

3.2.1. Tobermorite precipitation at the interface

The interface was still cohesive at 76 days, but not after 202 days (Fig. 4, right). After 202 days, the presence of a layer of white phases was observed with the naked eye on both sides of the interface. This brittle layer was determined to be a layer composed of C-S-H, tobermorite and calcite using SEM-EDS. This result was confirmed by XRD analysis (Figs. 4 and 5). Tobermorite is a crystalized calcium silicate hydrate structured in layers and is approximately denoted by C5S6H5 ($5CaO{\cdot}6SiO_2{\cdot}5H_2O$) in cement chemistry notation [32]. The Ca/Si and Al/Si ratios measured for the C-S-H by EDS were 0.83 and 0.18, respectively. Both ratios are consistent with tobermorite (Ca/Si = 0.83) and C-A-S-H. Nevertheless, the second one could also be consistent with decalcified C-S-H. The average width of this layer was approximately 100 µm at 415 days according to SEM-SE pictures (Fig. 5) and XRD measurements (Fig. 4, right).

3.2.2. Decalcification and carbonation of the cement paste

The consequences of a temperature increase on the mineralogy of a similar cement paste have been investigated previously [12]. At 20 °C, the cement paste of the present study was composed of portlandite, C-S-H, ettringite, and traces of calcite and katoite. After an increase in the temperature to 70 °C, ettringite was no longer observable and the amount of katoite increased. Based on previous studies, monosulfoaluminate was expected but was not detected. As shown in Fig. 4 (left), the XRD intensity profile of portlandite decreased from the interface to 250 µm at 76 and 202 days and to 400 µm at 415 days. In the youngest sample (76 days), the portlandite pattern was identified within the argillite on XRD profiles. Nevertheless, portlandite precipitation in the argillite while pouring the cement mix is unlikely, as the argillite was fully water-saturated. Due to the way that the XRD measurement was performed (see Section 2.3.2), the portlandite present within the cement paste was measured by transparency in the argillite close to the interface. Since it was an artefact, the measured intensities are represented with empty diamonds on the profile in Fig. 4.

The dissolution of portlandite was a rapid phenomenon, occurring as soon as the diffusion cells were sealed. Cement paste was decalcified at the interface as later confirmed by EDS analysis. The portlandite clusters, visible in the sound cement paste on the elementary maps of Ca (Fig. 4 right), were smaller and less abundant at the interface at the same depth. Carbonation of the cement paste by calcite precipitation was not observed at 76 days, but at 202 days, the presence of calcite was revealed in the first 150 µm from the interface and in the same area at 415 days (Fig. 4, left). At the interface, calcite crystals were unequally distributed for the two latest samples. Progressive carbonation of the C-S-H and tobermorite layer at the interface was also noticed (Fig. 6).

3.2.3. Argillite alteration: carbonation and disturbance of the clay minerals

Evolution of the argillite phases was followed by XRD analysis of the rock (Fig. 4 and Fig. S1 in the supplementary data file). Slight carbonation of the argillite occurred within the argillite as calcite precipitated. Signals of the argillite phases decreased at the interface. This general and concomitant decrease could be due to a matrix effect. Dissolution and precipitation probably occurred in this area and led to an evolution of the material structure. Therefore, it was difficult to fully determine an argillite disturbance only from the XRD analysis. Nevertheless, it seems reasonable that the argillite was altered over 100 µm from the interface and that this alteration mainly affected the clay phases. The kaolinite main peak intensity to illite main peak intensity

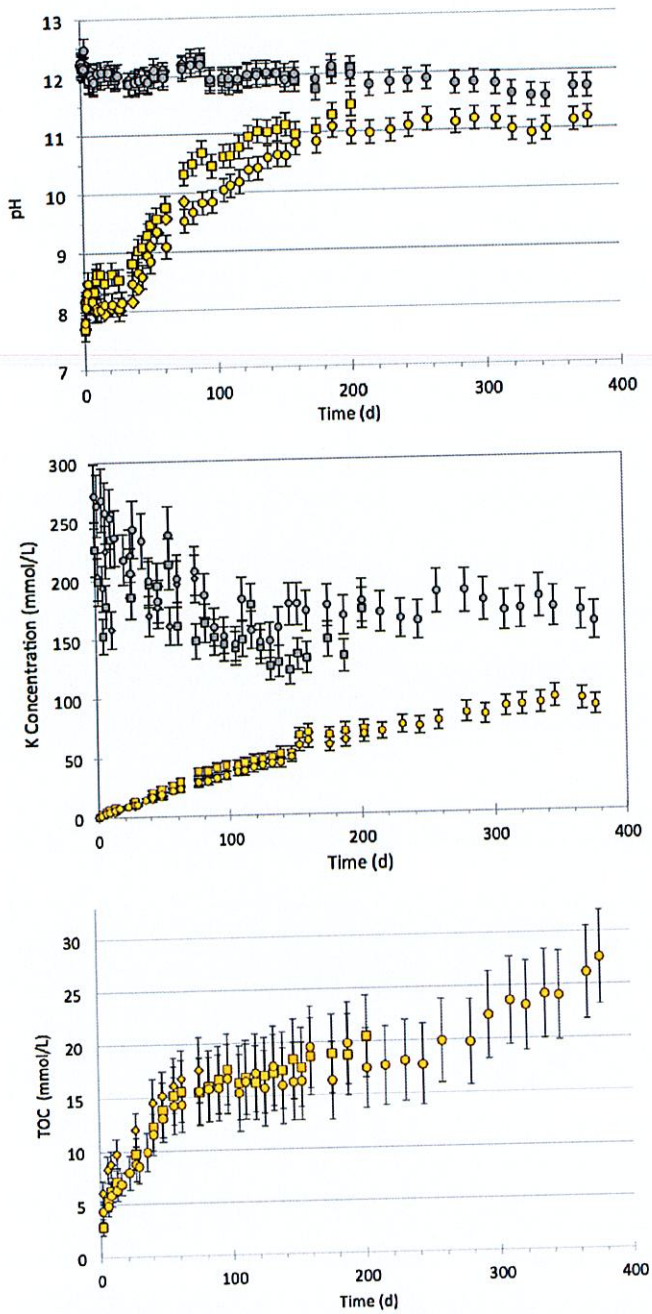

Fig. 3. Evolution over time of pH and K concentration in the alkaline reservoir (grey) and in the argillite reservoir (yellow). The cells were dismantled after 76 days (diamond), 202 days (square) and 415 days (disk). The dissolved total organic carbon was only measured in the argillite reservoir. (For interpretation of the references to colour in this figure legend, the reader is referred to the web version of this article.)

ratio was always higher than that in the sound argillite. This ratio progressively dropped below one moving towards the interface in the 76- and 415-day samples (Fig. 7). This evolution could be explained by kaolinite dissolution and to a lesser extent, illite may have precipitated. Dissolution of chlorite in the argillite could have occurred because its signal was no longer present more than 50 µm away from the interface at 415 days. Unfortunately, this conclusion could not be confirmed by the 202-day sample because no signal of chlorite in the sound argillite could be identified from the diffractogram background.

3.2.4. Macroporosity opening and texture evolution within the cement paste

Macroporosity was characterized using microtomography at a resolution of 1 µm. Therefore, only a portion of the largest pores was characterized (i.e., the pores larger than 1 µm). This is why the term macroporosity is used here, instead of porosity. Microtomography analyses were performed on the cement paste side of the separation surface between the materials. The argillite side of the separation surface was not analysed because the majority of the argillite pores has an average diameter smaller than 200 nm [33]. Nevertheless, some argillite was analysed in the cell that was dismantled after 76 days, as both materials remained stuck to each other. This proved by another means that the interface was contiguous (Fig. 8a). The pores hold air, which is less dense than other materials so that they appeared with the darker pixels on the microtomography pictures of Fig. 8. According to morphological considerations, a grey-level threshold was established to separate the porosity from the material phases. Using this threshold, the surface occupied by pores on each slice parallel to the interface was quantified to build macroporosity profiles (Fig. 8d).

On the microtomography slides (Fig. 8a), the brightest clusters, or the densest, were mainly composed of portlandite. Over time, the large and light clusters close to the interface decreased in size and their amount decreased compared to the sound material in a consistent manner with the XRD analysis presented before where portlandite dissolved over 400 µm. After 415 days, a macroporosity opening spread approximately 100 µm. Fig. 8 clearly shows the layer of C-(A)-S-H, tobermorite and calcite at the interface, as well as the physical separation between the argillite and the cement at 202 and 415 days.

3.2.5. Evolution of total connected porosity

Autoradiographs of the diffusion cells are shown in Fig. 9 (left). First, these results indicate that the C14-MMA intruded fully into the samples' pore space. Since the size of the MMA molecule is close to the size of water molecules, the MMA molecules can fully penetrate into the connected porosity. At 76 days, materials are still in direct contact with each other (cohesive interface). In front of cracks that were initially present within the argillite, at both 76 and 202 days, the porosity decreased sharply to 25% (green profile) in the cement paste. Cracks are preferential pathways for fluids, promoting the precipitation of phases such as calcite. The porosity decrease remained circumscribed and did not propagate along the interface. Therefore, the interface was cohesive throughout the whole experiment, and the interface opened after the alteration processes while dismantling and preparing the samples for analysis.

In the cement paste zones not affected by cracks, the porosity decreased from 33 to 29% over a 3-mm depth after 76 days. The porosity decrease extended deeper than the macroporosity opening detected by tomography and the mineralogical perturbations revealed by XRD. At 202 days, the porosity did not change. However, at 415 days, the cement paste porosity increased, with an average porosity value of 34% at the interface and maximum values of 37%. This reversible trend was not observed on the in situ sample, where a porosity decrease was still present after one year (Fig. 9, bottom graph). The mean porosity value obtained on the whole cement paste surface did not show any clear trend (Table 3). The high porosity found at the outer edges of the cement paste is probably an experimental artefact.

In the argillite, after 72 days, a thick band of lower porosity close to the interface was observed. In that area, the porosity decreased from 15% to 10%. This trend was not observed at 202 and 415 days, but a similar phenomenon occurred in the in situ samples that were aged for one year (Fig. 9, bottom graph). Further from the interface, the argillite porosity is significantly higher than the sound value (Fig. 9). Table 3 indicates that the total porosity constantly increased with experiment time (from 13 to 19% after 405 days). This could be due to uniform dissolution of the minerals induced by the highly alkaline plume that crossed the full sample (e.g., kaolinite dissolution, although not detected by XRD). The progressive release of dissolved organic matter

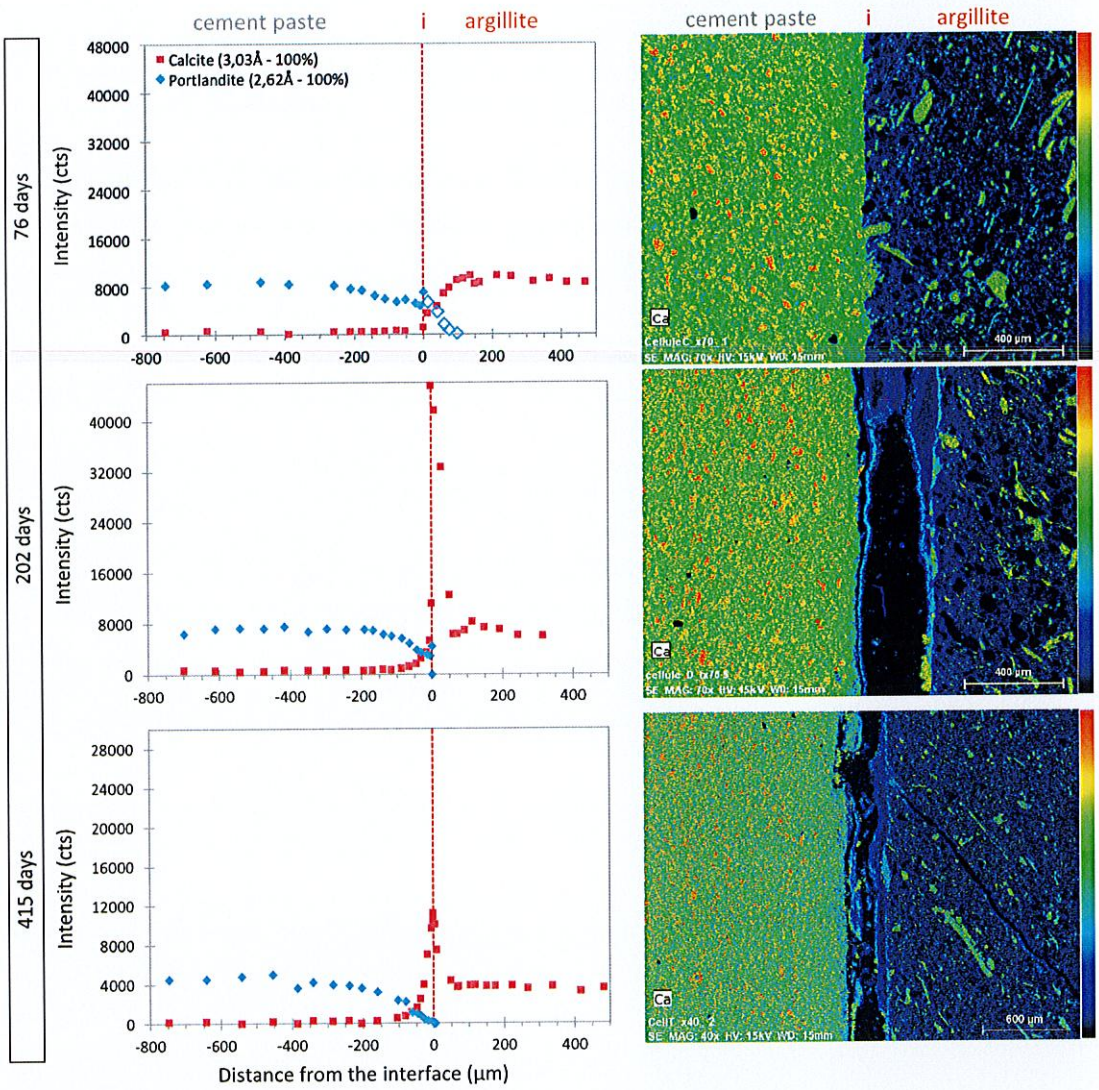

Fig. 4. Evolution over time of the XRD intensity profiles of portlandite (2.62 Å) and calcite (3.03 Å) over distance from the interface (left) and of the EDS elementary map of Ca (right); *i* stands for interface. Note: as the interface at 76 days was cohesive, XRD analyses were performed from the argillite through the coherent cement paste instead of starting from the interface plan. Elementary map scales provide the percentage of the element in each pixel, from 0% (i.e., absence) in blue to 100% in red (i.e., the pixel with the highest content in the considered element on the entire map). (For interpretation of the references to colour in this figure legend, the reader is referred to the web version of this article.)

from the clayey material (Fig. 3), concomitant to the propagation of the alkaline plume, has already been observed with the Tournemire argillite [15]. This plume of TOC could be an indicator of a strong perturbation of the argillite texture. The in situ sample also showed an increase in the argillite total porosity after one year (Fig. 9, bottom graph), although less intensely than in the cells.

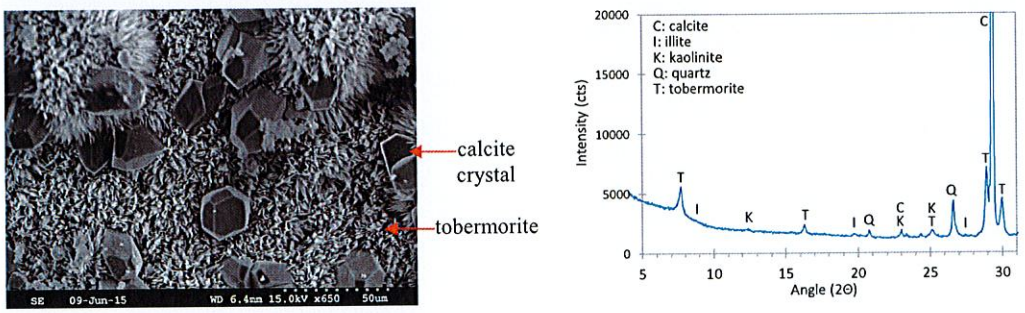

Fig. 5. SEM-SE image and XRD diffractogram of the cement/argillite interface on the argillite side at 202 days.

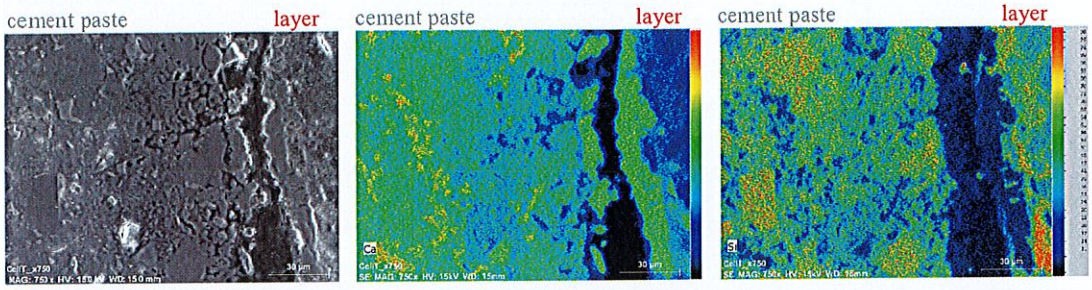

Fig. 6. SEM-SE picture and EDS element maps of Ca and Si at 415 days showing the carbonation of the C-(A-)S-H and tobermorite layers at the interface.

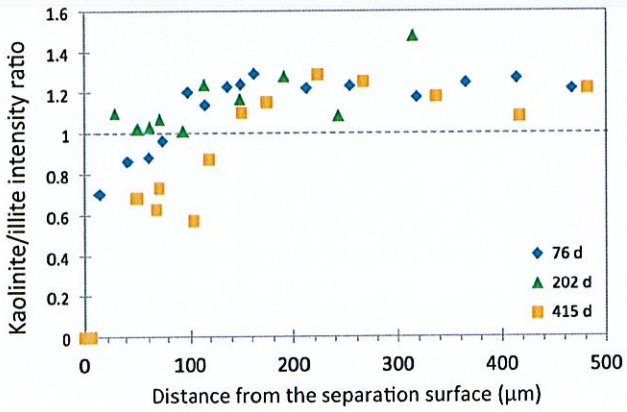

Fig. 7. Evolution of the ratio between the kaolinite main peak intensity to the illite main peak intensity using XRD data.

4. Discussion

4.1. Mineralogical and microstructural evolution

The deepest alteration process was portlandite dissolution within the cement paste and clay mineral disturbance within the argillite. The first mechanism occurred at a maximum depth of 400 µm, whereas the latter took place at 100 µm. C-S-H decalcification and carbonation also occurred over 150 µm in the cement paste. In the argillite, dissolution/precipitation processes affected kaolinite, chlorite and illite. At the interface, a layer of tobermorite, C-(A)-S-H and calcite was formed between 75 and 200 days and constituted a fragile plane with a loss of cohesion between cement and argillite. This layer was carbonated over time.

Porosity evolution was evaluated by X-ray microtomography and C14-PMMA autoradiography. Microtomography has a resolution of 1 µm only and macroporosity could be measured by the latter method. In the sound cement paste, the macroporosity was approximately 1 to 2% (i.e., only a small fraction of the total porosity). The macroporosity of the cement paste increased to over 100 µm thick after one year. This is directly related to the dissolution of portlandite clusters. Autoradiography facilitated a quantitative measurement of the total connected porosity with a nanometre-scale resolution. The total connected porosity decreased during the first 6 months.

This trend was reversed in the subsequent months, and the total connected porosity was clearly higher than the sound material value after 415 days. A porosity decrease was only noted in the in situ device [12], due to the precipitation of ettringite and calcite. Ettringite precipitation did not occur in the present cell experiments. The total

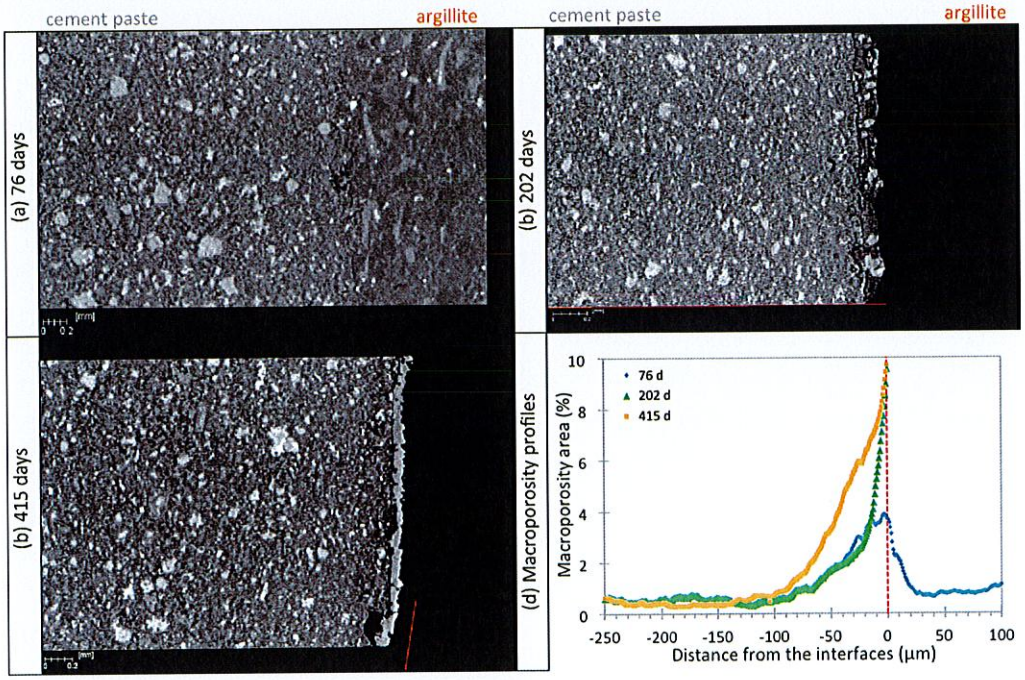

Fig. 8. Microtomography slides perpendicular to the interface of each diffusion cell. The bottom-right graph displays the macroporosity profiles built from the microtomography data.

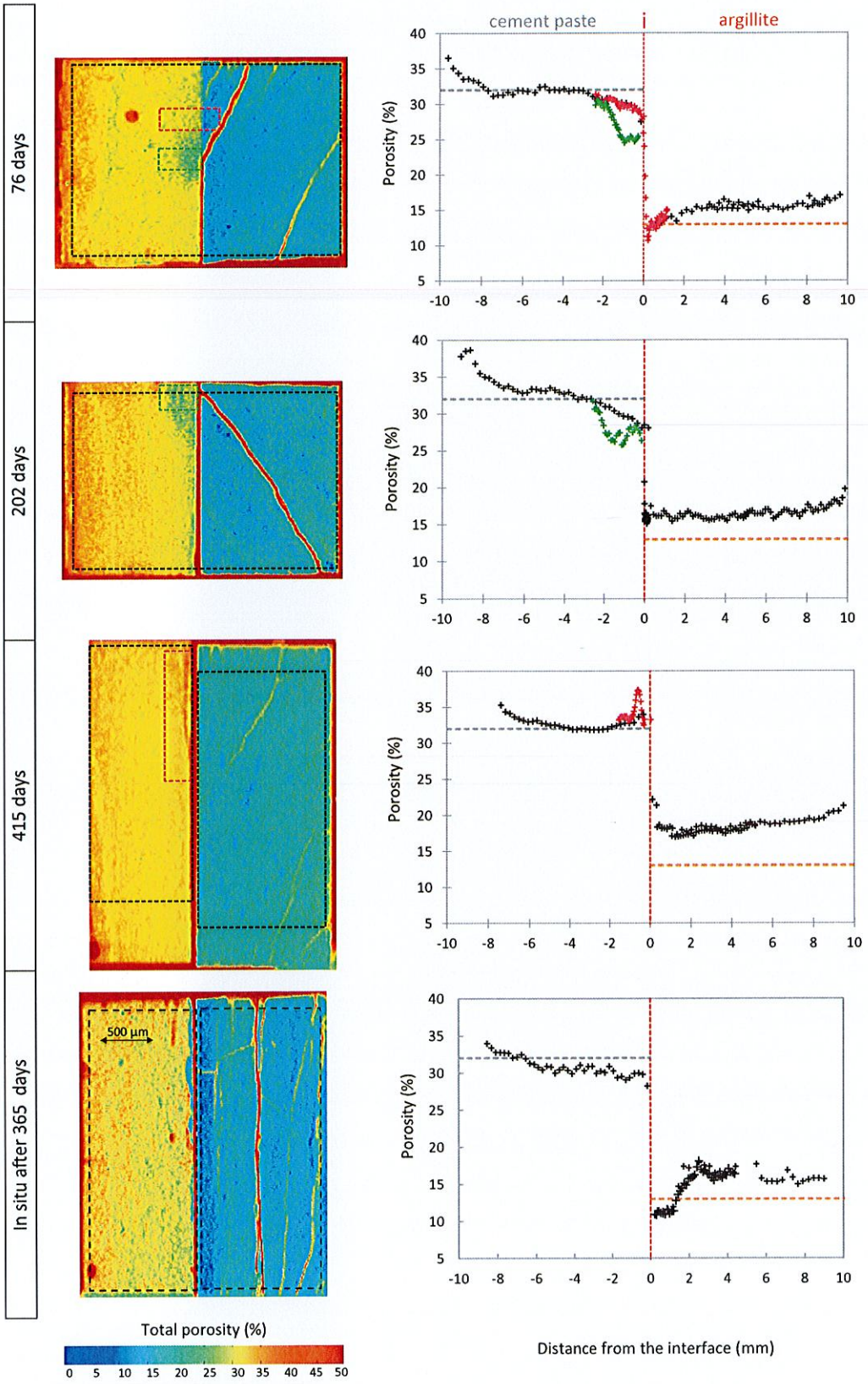

Fig. 9. Diffusion cell autoradiographs (left) and porosity profiles (right). Red areas correspond to high porosity and blue areas correspond to low porosity. Cement phases are on the left-hand side, argillite phases are on the right-hand side. Sample scale is approximately 2.0 cm × 1.5 cm. The total porosity of the sound materials measured by this technic is marked by the dotted lines on the graphs. Each dotted rectangle on the porosity maps represents the area where the profiles were determined. Rectangle colour on the left is linked to the same colour on the profiles on the right. (For interpretation of the references to colour in this figure legend, the reader is referred to the web version of this article.)

Table 3
Mean porosity value obtained by autoradiography on the entire sample surface (associated errors ± 1%).

Experiment time (day)	Clay porosity (%)	Cement porosity (%)
Sound materials	13	32
76	16	32
202	17	33
415	19	34

porosity of the cement paste decreased from 33% to 25% in front of argillite cracks. In the argillite, the total porosity increased over the total thickness of the argillite disk. This porosity opening constantly progressed over time. The increase in the total connected porosity within the argillite was likely due to the passage of the alkaline plume. However, the observations and analyses did not indicate such a deep and homogeneous perturbation of the rock. Only the cell dismantled at 76 days presented a band of lower porosity, in the argillite close to the interface, which is consistent with the in situ experiments.

The precipitation of ettringite and zeolite was not observed in the cement paste, in contrast to a similar experiment performed under in situ conditions [12]. The lack of ettringite and monosulfoaluminate could be explained by the relatively high amount of C4AF compared to C3A in the OPC used for the present experiment, which may have changed the equilibrium between ettringite and monosulfoaluminate at high temperatures at the benefit of katoite (see discussion in Section 3 of Lalan et al. [12]). In the diffusion cell, the pH in the argillite side reservoir progressively increased to reach 11 at 70 °C after 200 days (Fig. 3). It worth recalling that temperature shifts the pH to lower values and, therefore, that a pH of 11 at 70 °C corresponds to a hyperalkaline solution (a pH of 11.0 at 70 °C roughly corresponds to a pH of 12.4 at 20 °C in the present conditions). Fig. 10 shows that the zeolite K-phillipsite found in situ is not stable at pH 11 and that C-A-S-H can precipitate in equilibrium with tobermorite provided that the aluminium concentration is approximately $5 \times 10^{-4} m$ at 70 °C.

The pH remained relatively high in the cement paste, close to the pH value of the sound material. Therefore, the mineralogical and porosity disturbances within the cement paste progressed less deeply in the diffusion cells than in the in situ device [12].

4.2. Growth of tobermorite at the cement/argillite interface

Tobermorite-11A (i.e., structured in 11 Å thick layers) was identified by XRD. This mineral is a calcium silicate hydrate with a low Ca/Si ratio (0.83) and a well-defined crystal structure. It could crystallize from silicon released by the alteration of argillite (montmorillonite and kaolinite dissolution) and calcium released by decalcification of the cement phases (portlandite dissolution and C-S-H decalcification)

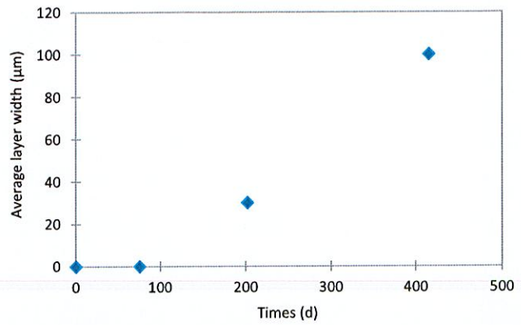

Fig. 11. Thickening over time of the layer made of a mix of C-S-H, tobermorite and calcite at the cement/argillite interface.

around the interface. At 20–25 °C, tobermorite-11A is more stable than C-S-H phases according to the stability diagram displayed in Fig. 10 based on thermodynamic equilibrium. Tobermorite is normally not a cement phase. That is, it is not a product of cement hydration at low temperatures. Its occurrence in the phase diagram at 25 °C is thermodynamically possible but kinetically inhibited. Tobermorite can be synthesized at 60 °C from CH and silicic acid in suspension [32]. At 70 °C, the stability diagram indicates that tobermorite is stable over a rather large pH range from 10 to 11.6 (at 25 °C the pH range would be 11–12.5). The zeolite K-phillipsite is more stable than tobermorite at lower pH values, and C-S-H with a Ca/Si ratio of 1.6 is more stable than tobermorite at the highest pH value. This fits well with the present observations where tobermorite precipitation took place at 70 °C, but only at the interface, and not within the hydrated cement paste.

Fig. 11 reports the temporal evolution of the width of the layer at the interface between the cement and the argillite. The layer required between 75 and 202 days to begin precipitating. This delay remains unexplained, but it could be due to the formation of an amorphous precursor not detected by XRD. The growth occurred in a single direction perpendicular to the disk section due to the cell geometry and was almost linear with time during the experiments. The growth rate was approximately 0.3 µm/d. This is consistent with the growth rate of 0.2 µm/d measured at the surface of a nuclear glass in contact with alkaline water at 90 °C, where the growth of the zeolite crystals was also perpendicular to the surface of the material [34].

4.3. Evolution of diffusion properties at the interface

The diffusion cells provided insights into the possible consequences of the formation of the secondary product layer at the interface on

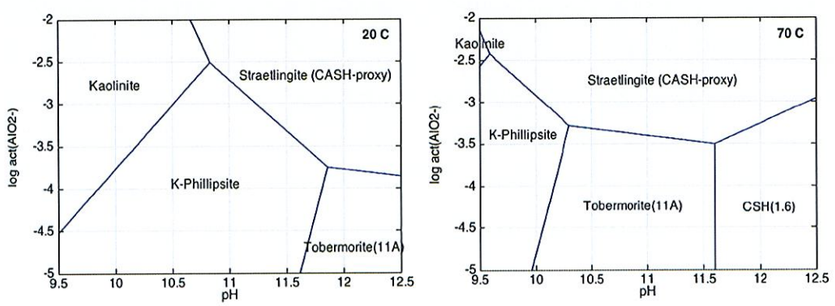

Fig. 10. Simplified phase diagrams of stability of the secondary phases CASH, tobermorite, and the potassic zeolite phillipsite, versus pH at 20 and 70 °C (act. $Ca^{2+} = 10^{-3}$, act. $K^{+} = 10^{-1}$, $[H_4SiO_4]_{total} = 10^{-3} m$).

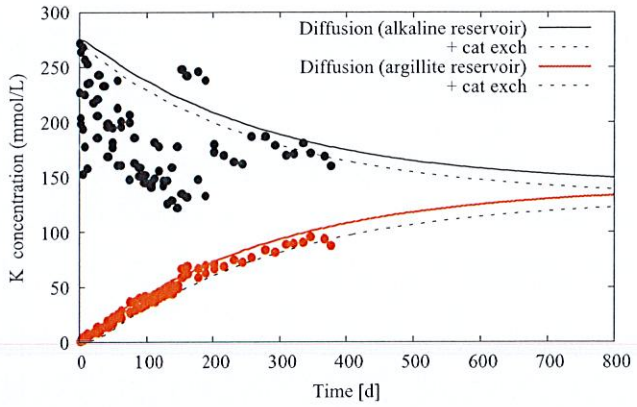

Fig. 12. Comparison of the experimental and calculated evolution over time of potassium concentration in both reservoirs of the diffusion cell, considering and not considering cation exchange; modelling is extended to 800 days to converge the results towards a stationary state.

diffusive transfers between cement and argillite. The cells were designed so that diffusive transport was predominantly 1D to simplify the modelling. To account for the temperature increase from 20 to 70 °C, the effective diffusion coefficient was multiplied by a factor 3 for the argillite, as found both for the Callovian-Oxfordian clay [35] and the Opalinus clay [36], and by a factor 10 for the OPC paste [37]. The modelling of potassium diffusion within the two materials corresponds well experimental data using such coefficients, particularly in the argillite reservoir (Fig. 12). It is worth noting that in the present experiment that has a high potassium concentration in the alkaline reservoir, potassium almost behaves similar to a perfect tracer. Taking into account that cation exchange does not significantly change the temporal evolution of potassium concentrations in the reservoirs (Fig. 12), the exchanger was saturated with potassium in less than 10 days. The lowest low-potassium concentrations in the alkaline reservoir (Fig. 12) correspond to the experiment cell that was dismantled after 202 days, as is shown in Fig. 3 (square symbols). The experiment conducted over the full 415 days was considered to be the most consistent reference for modelling. The temporal evolution of the potassium concentration did not indicate any decrease in the diffusion fluxes caused by porosity clogging.

The weak effect of the altered layer on diffusive transfer can be supported by a calculation assuming a diffusive system in a series (Fig. 13a). Indeed, in a first approximation, the sound cement paste (*cem*), the altered interface layer (*ail*) and the sound argillite (*arg*) can be considered as a three-layer system. By the analogy with electrical conductivities, such a system made of 3 parallel layers each with a diffusion coefficient D_i and a width w_i can be likened to a series circuit [38]. Then, the mean diffusion coefficient of the global system, $\overline{D_e}$, as a function of the thickness of the altered zone, can be calculated according to the following relationship

$$\frac{w_{tot}}{\overline{D_e}} = \frac{w_{cem}}{D_{e,cem}} + \frac{w_{ail}}{D_{e,ail}} + \frac{w_{arg}}{D_{e,arg}} \quad (1)$$

In the absence of an altered interface layer ($w_{ail} = 0$), the mean diffusion coefficient $\overline{D_e}$ is 3.3×10^{-11} m²/s at 70 °C ($w_{tot} = w_{cem} + w_{arg} = 10^{-2}$ m + 10^{-2} m = 2×10^{-2} m; $D_{e,cem} = 5.8 \times 10^{-11}$ m²/s; $D_{e,arg} = 2.3 \times 10^{-11}$ m²/s). In the present study, the thickness of the C-S-H layer at the interface was at most approximately 100 µm after 415 days (Figs. 6 and 11). Furthermore, C-S-H phases are not dense materials, but present a microporous structure allowing for mass transfer diffusion. The effective diffusion coefficient of synthetized C-S-H is approximately 10^{-10} m²/s, whatever the Ca/Si ratio, whereas it is approximately 3×10^{-11} m²/s inside a hydrated cement paste [9]. The former value is greater than the effective diffusion coefficient of the cement and argillite disks. The latter value is within the range of the effective diffusion coefficient of the cement and argillite disks. Therefore, in both cases, the influence on the mean diffusion coefficient remains negligible after one year of interaction, according to Eq. (1) (Fig. 13b).

Fig. 13b also indicates that the mean global coefficient decreases by less than one order of magnitude if the altered width is increased by one order of magnitude at a constant diffusion coefficient, or if the altered zone diffusion coefficient decreases by two orders of magnitude at a constant width. In contrast, if the altered zone diffusion coefficient is of the order of a non-porous calcite layer, i.e., 10^{-19} m²/s [39], the mean coefficient dramatically decreases by 6 to 7 orders of magnitude (Fig. 13b). This explains the clogging effect of calcite crust in experiments where cement pastes were immersed into carbonated water [40].

5. Conclusions

The diffusion cell with reservoirs has provided key information on the temporal evolution of pore water chemistry, secondary phase precipitation, porosity and diffusion properties. The main artefact of the present cell experiments was that the constant high-pH condition of the alkaline reservoir attenuated the alteration of the cement paste. Compared to the in situ sample, the decalcification front was half as deep as that in the cells, and the total porosity did not significantly decrease by carbonation after one year.

The present protocol where the cement paste is directly poured on the argillite generates a contiguous and homogeneous interface made of calcite/tobermorite/CASH layer. This corresponds to the formation of a

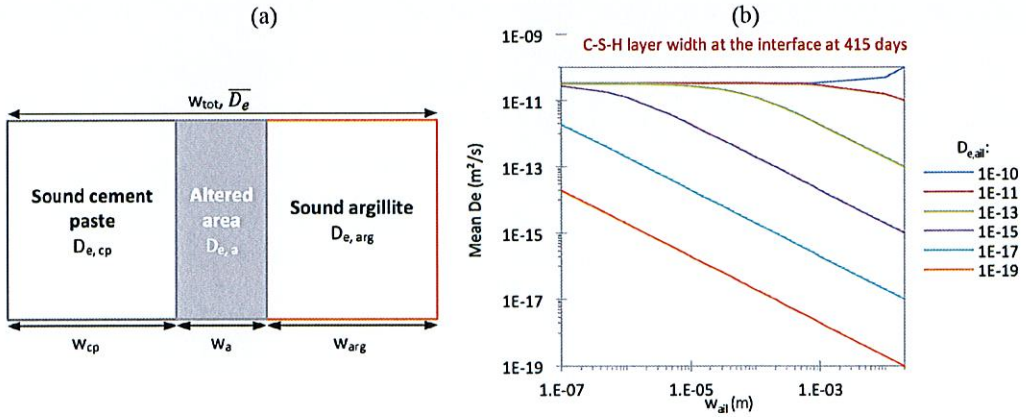

Fig. 13. Assuming a diffusive system in a series (a), the evolution of the mean effective diffusion coefficient of the system (b) is calculated (Eq. (1)) as a function of width (w_{ail}) and diffusion coefficient ($D_{e,ail}$) of the altered interface layer (*ail*).

brittle layer of secondary products with physical separation between the cement and clay observed after 6 months. The thickness of the layer (and probably its density) clearly increases with time. The layer of secondary products does not have a significant effect on diffusion after one year of interaction due to its rather small thickness and its microporous structure. In contrast, the formation of a non-porous calcite crust (in immersion tests or when a hardened cement disk is put in contact with the argillite disk) significantly slows diffusion and the progression of alteration fronts. A simplified modelling of clogging with Archie's law (i.e., porosity decrease due to tobermorite precipitation) is not applicable. A multi-scale description of the porosity is required.

Away from the interface, the investigation of the microstructure shows a closure of the total porosity in the cement paste (associated with carbonate precipitation) despite an opening in the macroporosity (linked to the dissolution of portlandite) over 400 µm after one year. In the argillite, the mineralogical alteration is restricted to 100 µm with a slight decrease in the total porosity. However, the alkaline plume clearly penetrated further away from the interface and progressively increased the rock porosity over 1 cm. Total porosity seems to be a finer indicator of chemical alteration than mineralogical analyses.

Compared to the results obtained at room temperature, a temperature of 70 °C has consequences on the mineralogy at the interface with the precipitation of the crystallized C-S-H tobermorite in the cell device and the formation of zeolite in situ, as well as the mineralogy of the cement paste with ettringite dissolution in the cells and in situ. The temperature increase also affected the mechanical strength of the interface, which became brittle over time. The total porosity at ambient temperature under interface conditions opens into the cementitious material [1], whereas it decreases at 70 °C. Consequently, the depth of mineralogical alteration is shallower at 70 °C than at 20 °C. Carbonation (in this joint interface system) is accentuated with temperature and counteracts the effect of decalcification. Therefore, it is not trivial to extrapolate the results obtained at room temperature to higher temperatures.

On-going analyses of similar interfaces subjected to 5 years of in situ interactions in the Tournemire URL could confirm whether the densification of the layer of secondary products increases with time to eventually lead to significant decreases in diffusional transfer. Investigating the effect of temperature on the evolution of interfaces between argillite and low-pH cement pastes is also in progress.

Supplementary data to this article can be found online at https://doi.org/10.1016/j.cemconres.2018.09.018.

Acknowledgements

We sincerely thank the reviewers for constructive criticisms and valuable comments. Christophe Morlot (Géoressources, Nancy, France) is also greatly acknowledged for his precious help for microtomography analyses and data processing, as well as the members of the LT2S laboratory (IRSN, France) for their analyses of the aqueous samples.

References

[1] S. Gaboreau, D. Prêt, E. Tinseau, F. Claret, D. Pellegrini, D. Stammose, 15 years of in situ cement–argillite interaction from Tournemire URL: characterisation of the multi-scale spatial heterogeneities of pore space evolution, Appl. Geochem. 26 (2011) 2159–2171.

[2] D. Bartier, I. Techer, A. Dauzères, P. Boulvais, M.-M. Blanc-Valleron, J. Cabrera, In situ investigations and reactive transport modelling of cement paste/argillite interactions in a saturated context and outside an excavated disturbed zone, Appl. Geochem. 31 (2013) 94–108.

[3] A. Jenni, U. Mäder, C. Lerouge, S. Gaboreau, B. Schwyn, In situ interaction between different concretes and Opalinus clay, Phys. Chem. Earth A/B/C 70–71 (2014) 71–83.

[4] A. Dauzères, G. Achiedo, D. Nied, E. Bernard, S. Alahrache, B. Lothenbach, Magnesium perturbation in low-pH concretes placed in clayey environment-solid characterizations and modeling, Cem. Concr. Res. 97 (2016) 61–72.

[5] U. Mäder, A. Jenni, C. Lerouge, S. Gaboreau, S. Miyoshi, Y. Kimura, V. Cloet, M. Fukaya, F. Claret, T. Otake, M. Shibata, B. Lothenbach, 5-year chemico-physical evolution of concrete–claystone interfaces, Mont Terri rock laboratory (Switzerland), Swiss J. Geosci. 110 (2017) 307–327.

[6] A. Dauzeres, P. Le Bescop, P. Sardini, C. Cau Dit Coumes, Physico-chemical investigation of clayey/cement-based materials interaction in the context of geological waste disposal: experimental approach and results, Cem. Concr. Res. 40 (2010) 1327–1340.

[7] R. Fernández, J. Cuevas, L. Sánchez, R.V. de la Villa, S. Leguey, Reactivity of the cement–bentonite interface with alkaline solutions using transport cells, Appl. Geochem. 21 (2006) 977–992.

[8] D. Read, F.P. Glasser, C. Ayora, M.T. Guardiola, A. Sneyers, Mineralogical and microstructural changes accompanying the interaction of boom clay with ordinary Portland cement, Adv. Cem. Res. 13 (2001) 175–183.

[9] N. Seigneur, A. Dauzeres, M. Voutilainen, V. Detilleux, P.E. Labeau, A. Dubus, Numerical representative elementary volume generation of a simplified cement paste and estimation of its diffusivity and comparison with dedicated experiments, J. Porous Media 20 (2017) 1–18.

[10] O. Bildstein, F. Claret, Stability of clay barriers under chemical perturbations, in: C. Tournassat, C.I. Steefel, I.C. Bourg, F. Bergaya (Eds.), Natural and Engineered Clay Barriers, Developments in Clay Science, 6 Elsevier, Amsterdam, 2015.

[11] L. De Windt, D. Pellegrini, J. van der Lee, Coupled modeling of cement/claystone interactions and radionuclides migration, J. Contam. Hydrol. 68 (2004) 165–182.

[12] P. Lalan, A. Dauzères, L. De Windt, D. Bartier, J. Sammaljärvi, J.-D. Barnichon, I. Techer, V. Detilleux, Impact of a 70 °C temperature on an ordinary Portland cement paste/claystone interface: an in situ experiment, Cem. Concr. Res. 83 (2016) 164–178.

[13] L. De Windt, J. Cabrera, J.-Y. Boisson, Radioactive waste containment in indurated claystones: comparison between the chemical containment properties of matrix and fractures, in: R. Metcalfe, C.A. Rochelle (Eds.), Chemical Containment of Waste in the Geosphere, 157 Geological Society of London Special Publication, 1999, pp. 167–181.

[14] J. Tremosa, D. Arcos, J.M. Matray, F. Bensenouci, E.C. Gaucher, C. Tournassat, J. Hadi, Geochemical characterization and modelling of the Toarcian/Domerian porewater at the Tournemire underground research laboratory, Appl. Geochem. 27 (2012) 1417–1431.

[15] C. Chautard, A. Ritt, L. De Windt, M. Libert, D. Stammose, Characterization of low-molecular-weight organic acids isolated from the Toarcian argillite pore water (Tournemire site, France), Compt. Rendus Geosci. 347 (2015) 77–83.

[16] C. Wittebroodt, S. Savoye, B. Frasca, P. Gouze, J.L. Michelot, Diffusion of HTO, $^{36}Cl^-$ and $^{125}I^-$ in Upper Toarcian argillite samples from Tournemire: effects of initial iodide concentration and ionic strength, Appl. Geochem. 27 (2012) 1432–1441.

[17] S. Motellier, I. Devol-Brown, S. Savoye, D. Thoby, J.C. Alberto, Evaluation of tritiated water diffusion through the Toarcian clayey formation of the Tournemire experimental site (France), J. Contam. Hydrol. 94 (2007) 99–108.

[18] C. Chautard, J.E. Lartigue, M. Libert, F. Marsal, L. De Windt, An integrated experiment coupling iron/argillite interactions with bacterial activity, Procedia Chem. 7 (2012) 641–646.

[19] B. Albert, Altération des matrices cimentaires par des eaux de pluie et des eaux sulfatées: approche expérimentale et thermodynamique, (2002) (Thèse de l'Ecole Nationale Supérieure des Mines de Saint-Etienne).

[20] G. Le Saout, T. Füllmann, V. Kocaba, K. Scrivener, Quantitative study of cementitious materials by X-ray diffraction/Rietveld analysis using an external standard, 12th International Congress on the Chemistry of Cement, July 2007, Montréal (Canada), 2008.

[21] A. Blumstein, Polymerization of adsorbed monolayers. I. Preparation of clay–polymer-complex, J. Polym. Sci. A 3 (1965) 2653–2664.

[22] A. Blumstein, Polymerization of adsorbed monolayers. II. Thermal degradation of the inserted polymer, J. Polym. Sci. A 3 (1965) 2665–2672.

[23] K.-H. Hellmuth, M. Siitari-Kauppi, A. Lindberg, Study of porosity and migration pathways in crystalline rock by impregnation with 14C-polymethylmethacrylate, J. Contam. Hydrol. 13 (1993) 403–418.

[24] K.-H. Hellmuth, S. Lukkarinen, M. Siitari-Kauppi, Rock matrix studies with carbon-14-polymethylmethacrylate (PMMA); method development and applications, Isot. Environ. Health Stud. 30 (1994) 47–60.

[25] J. Sammaljärvi, L. Jokelainen, J. Ikonen, M. Siitari-Kauppi, Free radical polymerization of methyl methacrylate with thermal initiator in brick and Grimsel granodiorite, Eng. Geol. 135 (2012) 52–59.

[26] J. Sammaljärvi, M.S. Rama, J. Ikonen, E. Muuri, K.H. Hellmuth, M. Siitari-Kauppi, Free radical polymerisation of methacrylates with thermal initiator in clay rock, Eng. Geol. 210 (2016) 70–83.

[27] S. Sammartino, M. Siitari-Kauppi, A. Meunier, P. Sardini, A. Bouchet, E. Tevissen, An imaging method for the porosity of sedimentary rocks: adjustment of the PMMA method – example of a characterization of a calcareous shale, J. Sediment. Res. 72 (2002) 937–943.

[28] M. Siitari-Kauppi, Development of 14-C-polymethylmethacrylate method for the characterisation of low porosity media - application to rocks in geological barriers of nuclear waste storage, Report Series in Radiochemistry 17/2002, 2002.

[29] J. van der Lee, L. De Windt, V. Lagneau, P. Goblet, Presentation and application of the reactive transport code HYTEC, Dev. Water Sci. 47 (2002) 599–606.

[30] P. Blanc, A. Lassin, P. Piantone, M. Azaroual, N. Jacquemet, A. Fabbri, E.C. Gaucher, Thermoddem: a geochemical database focused on low temperature water/rock interactions and waste materials, Appl. Geochem. 27 (2012) 2107–2116.

[31] E. Jobard, Modélisation expérimentale du stockage géologique du CO_2: étude particulière des interfaces entre ciment de puits, roche reservoir et roche couverture (PhD thesis), Université de Lorraine, France, 2013.

[32] H.F.W. Taylor, Cement Chemistry, 2nd edition, Thomas Telford Publishing, 1997.
[33] M.V. Altinier, Etude de la composition isotopique des eaux porales de l'argilite de Tournemire: inter-comparaison des méthodes de mesure et relations avec les paramètres pétrophysiques (PhD thesis), Paris 11, France, 2006.
[34] S. Gin, P. Jollivet, M. Fournier, C. Berthon, Z. Wang, A. Mitroshkov, Z. Zhu, J.V. Ryan, The fate of silicon during glass corrosion under alkaline conditions: a mechanistic and kinetic study with the international simple glass, Geochim. Cosmochim. Acta 151 (2015) 68–85.
[35] S. Savoye, F. Goutelard, C. Beaucaire, Y. Charles, A. Fayette, M. Herbette, Y. Larabi, D. Coelho, Effect of temperature on the containment properties of argillaceous rocks: the case study of Callovo–Oxfordian claystones, J. Contam. Hydrol. 125 (2011) 102–112.
[36] L.R. Van Loon, W. Müller, K. Iijima, Activation energies of the self-diffusion of HTO, $^{22}Na^{+}$ and $^{36}Cl^{-}$ in a highly compacted argillaceous rock (Opalinus clay), Appl. Geochem. 20 (2005) 961–972.
[37] C. Page, N. Short, A. El Tarras, Diffusion of chloride ions in hardened cement pastes, Cem. Concr. Res. 11 (1981) 395–406.
[38] J. Crank, The Mathematics of Diffusion, 2d ed., Clarendon Press (UK), Oxford, 1975.
[39] S. Liu, D. Jacques, J. Govaerts, L. Wang, Conceptual model analysis of interaction at a concrete–boom clay interface, Phys. Chem. Earth A/B/C 70 (2014) 150–159.
[40] A. Dauzères, Etude expérimentale et modélisation des mécanismes physico-chimiques des interactions béton-argile dans le contexte du stockage géologique des déchets radioactifs (PhD thesis), Université de Poitiers, France, 2010.